ACS APPLIED MATERIALS & INTERFACES

www.acsami.org

Research Article

Optical Multisensor Array with Functionalized Photonic Droplets by an Interpenetrating Polymer Network for Human Blood Analysis

Ye-Ji Kim and Soo-Young Park*

Cite This: https://dx.doi.org/10.1021/acsami.0c15718

Read Online

ACCESS | Metrics & More | Article Recommendations | Supporting Information

ABSTRACT: Photonic solid-state cholesteric liquid crystal (CLC_{solid}) droplets intertwined with a poly(acrylic acid) (PAA) network that has an interpenetrating polymer network (IPN) structure (referred to as photonic IPN $CLC_{solid-PAA}$ droplets) were used as individual sensors in the dots of a PAA-patterned array film after functionalization via immobilization of the receptors and a metal-ion treatment. The photonic IPN $CLC_{solid-PAA}$ droplets in the PAA-patterned array film were pH-responsive and showed an observable change in the reflected central color. This "smart" property, coupled with the photonic color response, makes these devices ideal photonic sensors. The immobilization of urease and phenylboronic acid on the PAA network allowed for the application of several 10 μm photonic IPN $CLC_{solid-PAA}$ droplets to the optical photonic biosensors through facilitated volumetric changes in the PAA network in response to urea and glucose analytes, with high selectivity for major components in human serum, acceptable sensitivity for use with human serum, and extreme stability due to a solid-state structure. The blueshift of the reflected color of the KOH-treated photonic IPN $CLC_{solid-PAA}$ droplets could be used for divalent metal-ion detection. The compartmentalized photonic IPN $CLC_{solid-PAA}$ droplets in the patterned array film could be used for multiple detection applications, as evidenced by the ability to conduct pH, divalent metal ion, urea, and glucose detections in one patterned array film. This new platform opens the door for many interesting applications with numerous combinations of responsive hydrogel matrices and receptors.

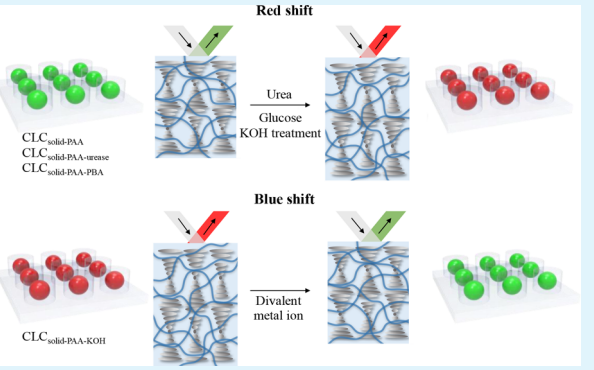

KEYWORDS: *photonic array, interpenetrating polymer network, microfluidics, biosensor, cholesteric liquid crystal*

INTRODUCTION

Artificial photonic crystals are of research interest because of their ability to control light via the photonic bandgap (PBG). These periodic arrays of dielectric materials can be generated via several methods, including multilayer lithography,[1] multibeam holographic lithography,[2,3] optical interference methods,[4] colloidal self-assembly,[5−8] and helicoidal self-assembly with cholesteric liquid crystals (CLCs).[9−12] The helicoidal photonic structure of CLC can be produced by mixing nematic LC with a chiral dopant, and the reflected color of CLC can be easily tuned by adjusting the concentration of the mixed chiral dopant. A complete solid-state CLC (CLC_{solid}) can be made from reactive mesogen mixtures doped with the chiral dopant after UV curing, and chiral dopant extraction occurs when nonreactive chiral dopants are used.[8,13,14] The photonic CLC_{solid} film's structure is ideal for use as a sensor because it facilitates a reflected color change when the helicoidal pitch adjusts in response to external stimuli. A distinct, vivid, and uniform reflected color can be seen in the flat film when the layers formed by its helicoidal structure are perfectly parallel to the film's surface. One of the disadvantages of using the flat film as a sensitive optical sensor lies in the fact that the reflected color changes according to the direction of the incident beam, as per Bragg's law. The small (i.e., several tens of μm in diameter) photonic spherical droplet, which exhibits a planar anchoring condition that can be easily controlled using surface-coating materials such as poly(vinyl alcohol) (PVA), circumvents this issue of incident beam-dependent variance in the reflected color because its helicoidal axis follows the radial direction; this, in turn, causes the tangential reflection plane to be aligned perpendicular to the incident beam regardless of the direction of the incident beam as shown in Figure S1. This small photonic droplet can be used as an optical sensor when the pitch of the helix changes in response to external stimuli.[15−18] These smart properties can only be triggered when responsive groups are incorporated into the structure of CLC_{solid} via chemical modification or the inclusion of reactive

Received: September 1, 2020
Accepted: September 25, 2020

mesogens equipped with responsive groups. Aside from being complex, labor-intensive, and time-consuming, the chemical modification of these CLC_{solid} droplets does not always lead to the successful incorporation of the desired responsive group due to the scarcity of the corresponding reactive mesogens.

Smart interpenetrating polymer networks (IPNs) have been incorporated in CLC_{solid} structures.[19−21] One such reported photonic IPN structure consists of two intertwined CLC_{solid} and hydrogel networks that are responsible for the reflected photonic color and volume changes observed in response to external stimuli, respectively.[15−18,22] The uniformly sized CLC_{solid} droplets, which are typically produced via a microfluidic method, can be functionalized by incorporating this IPN structure via the infiltration of hydrogel monomers with crosslinkers into the space created by the extracted dopants. Subsequent ultraviolet (UV) or thermal curing produces an intertwined structure. These photonic IPN CLC_{solid} droplets with an intertwined PAA network (abbreviated as $CLC_{solid-PAA}$ droplet) can be used as pH-responsive sensors since the intertwined PAA is a weakly anionic polyelectrolyte that undergoes pH-dependent volume changes. This responsiveness is particularly important in biosensor applications since most biological systems are influenced by changes in the prevailing pH conditions. When the CLC_{solid} droplets are placed in the hydrogel monomer mixture to make the photonic IPN structure, the monomer mixture is cured both inside and outside the CLC_{solid} droplets. Thus, the formation of the photonic IPN structure inside the CLC_{solid} droplet and the solid-state hydrogel matrix structure outside the CLC_{solid} droplet occurs simultaneously. When the hydrogel mixture containing the photonic IPN CLC_{solid} droplets is filled in a designated container and then solidified via UV or thermal curing, an arbitrarily shaped matrix is formed. These matrix-containing photonic IPN CLC_{solid} droplets provide various platforms for the sensors. For example, the patterned dots in the array film can be used either for multiple detection purposes or as a patch on human skin. Zhang et al. reported that stimuli-responsive polyelectrolyte complexes were structured into micropillar arrays to monitor the pH variation and the presence of calcium ions based on reversible swelling/shrinking behaviors of the polymers.[23,24] When illuminated by a laser light, the microarray films generated diffraction patterns that can reflect and magnify variations of the periodical microstructure induced by surrounding invisible parameters in real time. However, sensor arrays have not been used, in combination with multivariate data analysis, to increase the sensitivity toward isolated species and for the quantification of the amount of a single species. Recently, Ko et al. studied polyaniline/polyethylene glycol (PANI/PEG) composite arrays for colorimetric sensor applications. They used PANI/PEG composite arrays as a pH sensitive indicator to detect bacterial growth because of their colorimetric responses to pH changes. However, they have not developed the sensing system with multiple analytes.[25]

The photonic IPN $CLC_{solid-PAA}$ droplets can be applied to biosensors when the intertwined PAA hydrogel can respond to biological events. Many electrochemical methods have been reported for use in biosensor applications. However, electrochemical sensors are particularly complex to operate because the electrodes are connected to a small test site through conducting lines.[26,27] Thus, constructing simple and cost-effective optical biosensors that possess direct observation capabilities without the need for sophisticated analytical instruments is of keen interest to researchers. To this end, photonic IPN $CLC_{solid-PAA}$ films have been applied to enzyme-based optical biosensors. Here, the carboxylic group-mediated immobilization of the enzymes via coupling reactions with 1-ethyl-3-(3-dimethylaminopropyl)carbodiimide (EDC) changed the reflected color of the photonic IPN $CLC_{solid-PAA}$ film.[15,19] Previous studies on photonic IPN $CLC_{solid-PAA}$ array films featured the carboxylic group-mediated immobilization of urease and the selective reaction of urea, which resulted in higher pH values due to the production of hydroxyl ions, an expanded PAA network, increased pitch of the CLC_{solid}, and changes in the reflected color. Nonenzymatic receptors can also be applied to photonic IPN $CLC_{solid-PAA}$ films. Here, aminophenylboronic acid (APBA) was immobilized in the PAA network via EDC coupling.[15] Phenylboronic acid (PBA) could selectively bind glucose, and the complexation reaction between PBA and glucose generated the Donnan osmotic pressure that resulted in volumetric changes in the PAA network. These changes altered the pitch and the reflected color of the photonic IPN $CLC_{solid-PAA}$ array film. The resulting PBA-immobilized IPN $CLC_{solid-PAA}$ (abbreviated as $CLC_{solid-PAA-PBA}$) film sensors facilitated the screening of various glucose concentrations without the need for sophisticated analytical instruments and electrical components.

Since metal ions in biofluids serve as essential biomarkers for several diseases, their detection in human biofluids is of paramount importance for diagnostic purposes. Here, the extremely reactive carboxylic groups of PAA are ionized at high pH levels and can form complexes with these metal ions. The resulting complex, which consists of monovalent ions such as K^+ and Na^+, can block hydrogen bonding between the carboxylic groups, swell the PAA network, increase the helicoidal pitch, and redshift the reflected color. On the other hand, complexes containing divalent ions (Ms) such as Ca^{2+} and Mg^{2+} form a bridged -COO−M−OOC− structure that inhibits swelling of the PAA network, decreases the helicoidal pitch, and blueshifts the reflected color. This phenomenon is particularly noticeable when relatively large amounts of Ca^{2+} and Mg^{2+} ions (which are detectable with the developed photonic IPN $CLC_{solid-PAA}$ system) are present in biofluids.[28−30] Swollen (red-colored) photonic IPN $CLC_{solid-PAA}$ droplets pretreated with monovalent ions (e.g., K^+) can undergo a blueshift when treated with Ca^{2+} and Mg^{2+} ions. This occurs because the divalent ions can replace the monovalent ions due to their higher reactivity and their proclivity to react with carboxylate ions.[18,31] Thus, the monovalent ion-treated photonic IPN $CLC_{solid-PAA}$ droplets can even be used to detect divalent ions.

In this work, PAA-patterned dot array films containing photonic IPN $CLC_{solid-PAA}$ droplets in the dots were prepared using a polydimethylsiloxane (PDMS) mold. These prepared photonic IPN $CLC_{solid-PAA}$ droplets were employed as biosensors for the detection of divalent metal ions, urea, and glucose in model studies. This patterned array film impregnated with photonic IPN $CLC_{solid-PAA}$ droplets provides a new broad-range biosensor platform that can be distinguished via the compartmentalization of the photonic IPN CLC_{solid} droplets in the array dots and/or the initial reflected color controlled by adjusting the concentration of the chiral dopant.

https://dx.doi.org/10.1021/acsami.0c15718
ACS Appl. Mater. Interfaces XXXX, XXX, XXX−XXX

Scheme 1. Schematics of the Preparation of Photonic IPN $CLC_{solid-PAA}$ Droplets in the PAA-Patterned Array Film

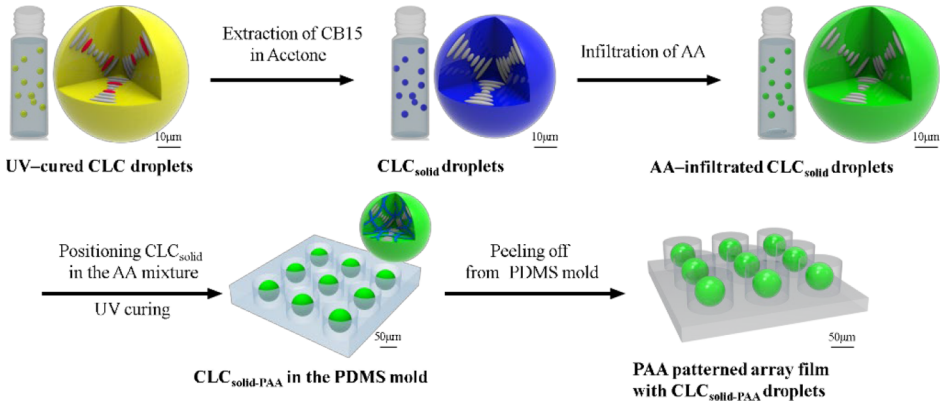

EXPERIMENTAL SECTION

Materials. Reactive liquid crystal mixture RMM727 (Merck, UK), (*S*)-4-cyano-4′-(2-methylbutyl)biphenyl (CB15, Synthon, Germany), glycerin (Duksan, South Korea), poly(vinyl alcohol) (PVA, Yakuri, Japan), trichloro(1H,1H,2H,2H-perfluorooctyl)silane (PFOTS, 97%, Merck, USA), tetraethyl orthosilicate (TEOS, TCI Chemicals, Japan), 3-(trimethoxysilyl)propyl methacrylate (TMSPMA, 98%, Merck, USA), bare glass slides (Marienfeld, Germany), acrylic acid (AA, Junsei, Japan), a Irgacure 500 photoinitiator (Ciba Inc., Switzerland), acetone (Duksan, South Korea), Poly/Bed 812 (Epon, Polysciences, USA), dodecenylsuccinic anhydride (DDSA, Polysciences, USA), nadic methyl anhydride (NMA, Polysciences, USA), 2,4,6-tris-(dimethylaminomethyl)phenol (DMP, Polysciences, USA), potassium hydroxide (KOH, Duksan, South Korea), anhydrous calcium chloride ($CaCl_2$, Yakuri, Japan), nitric acid (HNO_3, Duksan, South Korea), poly(dimethylsiloxane) (PDMS, Sylgard 184 silicone elastomer kit, Dow Corning, USA), *N*-hydroxysuccinimide (NHS, Merck, USA), *N*-(3-dimethylaminopropyl)-*N*′-ethylcarbodiimide hydrochloride (EDC•HCl, Merck, USA), pH buffer solution (Samchun, South Korea), rhodamine 6G (TCI, Japan), urea (Merck, USA), urease (Merck, USA), glucose (Merck, USA), cholesterol (Merck, USA), L-ascorbic acid (Merck, USA), uric acid (Merck, USA), copper(II) nitrate trihydrate ($Cu(NO_3)_2{\cdot}3H_2O$, Junsei, Japan), zinc nitrate hexahydrate ($Zn(NO_3)_2{\cdot}6H_2O$, Merck, USA), magnesium nitrate hexahydrate ($Mg(NO_3)_2{\cdot}6H_2O$, Merck, USA), sodium nitrate ($NaNO_3$, Duksan, South Korea), human serum (Merck, USA), and iron(II) chloride tetrahydrate ($FeCl_2{\cdot}4H_2O$, Samchun, South Korea) were purchased from the aforementioned suppliers and used as received. Deionized (DI) water was purified using a μPure RO reverse-osmosis system (Romax, South Korea).

DI water was used for all experiments unless otherwise stated. Predetermined amounts of RMM727 and CB15 were mixed and magnetically stirred at 60 °C for 12 h. The resulting transparent chiral mixture became milky after thoroughly stirring and cooling to 25 °C.

Preparation of Patterned Photonic CLC_{solid} Droplets in the PAA Matrix. Uniform CLC_{solid} droplets were prepared via the reported method in a microfluidic channel with omnidirectional UV curing of the RMM/CB15 mixture (Figure S2) and chiral dopant extraction.[16,32,33] An omnidirectional UV curing process was adopted to prevent the formation of asymmetric photonic structures that were influenced by the direction of UV irradiation. This was because unidirectional irradiation causes phase separation to occur on the UV-shed side first, resulting in the migration of the phase-separated chiral dopant to the other side of the UV impact zone during the curing process. This would blueshift the reflected color on the other side of the CLC droplet's hemisphere due to its higher chiral dopant content. Thus, omnidirectional UV curing circumvented this issue. The detailed experimental setup and methodology can be found in Text S1 and Figure S3 of the Supporting Information.

The amount of chiral dopant (ϕ) was fixed at 29.4 wt % unless otherwise mentioned. The reflected central color of the CLC_{solid} droplet at ϕ = 29.4 wt % shows a blue reflection in the dried state. Figure S4a displays the scanning electron microscopy (SEM) image of the cross-sectional surface of the CLC_{solid} droplets after CB15 extraction and drying. Compact structures with perfect concentric rings and no voids were observed, indicating that the CLC helical structure was maintained after UV curing and CB15 extraction. This intact CLC photonic structure may be the result of the complete miscibility of RMM and CB15, as well as the homogeneous UV curing process. The concentric rings represented the helical structure with layer spacing that corresponded to the helical pitch (P). The measured P of 364 nm (which is twice the distance between the adjacent lines) gave the wavelength at PBG (λ_{PBG}) of 473 nm; this was calculated using $\lambda_{PBG} = nP$, where n (1.3) was the average reflective index.[16] The λ_{PBG} at 473 nm was in the blue range and close to the observed color.

Scheme 1 shows the preparation of the photonic IPN $CLC_{solid-PAA}$ droplets in the dots of the PAA-patterned array film that was replicated from the PDMS mold. The PDMS mold was prepared using a common photoresist method. Briefly, SU80 was coated on a silicon wafer with a thickness of 100 μm and was patterned using UV with a photomask containing transparent 200 × 200 array circles (with a diameter of 100 μm) separated by 200 μm center-to-center in a square with a black background. The pattern developed on the silicon wafer had cylindrical poles with a height of 100 μm. The PDMS precursor was poured into a Petri dish containing the silicon wafer on the bottom. After the air bubbles were removed using a vacuum pump, the PDMS precursor was UV-cured using an Innocure 5000 (Lichtzen, South Korea). The PDMS mold, which was peeled from the patterned silicon wafer, had cylindrical holes (Figure S5). The prepared CLC_{solid} droplets were dispersed in a mixture containing AA monomers (98.5 wt %), TPGDA (0.5 wt %), and Irgacure 500 (1 wt %). The combined CLC_{solid} droplet–AA mixture was poured in the PDMS mold, which had been treated with O_2 plasma for 5 min, before being left for 5 min to allow the CLC_{solid} droplets to settle in the PDMS holes and pressed with a glass slide on top.

The blue color of the central reflection of the CLC_{solid} droplets became green as the CLC_{solid} droplets dispersed in the AA mixture were omnidirectionally UV-cured using a specially designed UV curing machine (Figure S2) with an intensity of 250 $\mu W{\cdot}cm^{-2}$ to ensure uniform curing. The dotted PAA-patterned array film containing the photonic IPN $CLC_{solid-PAA}$ droplets was peeled from the PDMS mold.

$CLC_{solid-PAA-urease}$ Droplets for Urea Biosensors. The immobilization of urease on the intertwined PAA network was tracked by labeling urease with rhodamine 6G via the following method. The aqueous urease solution (1 wt %, 5 mL) was mixed with an aqueous EDC/NHS (1/2 v/v, 0.2 M/0.2 M, 1 mL) solution by magnetic stirring for 1 h to activate urease. The EDC-activated urease aqueous solution (1 wt %, 6 mL) was mixed with rhodamine 6G (0.5 mg) by magnetic stirring for 10 h. The rhodamine 6G-immobilized urease (rho–urease) was purified by adding an aqueous ammonium

https://dx.doi.org/10.1021/acsami.0c15718
ACS Appl. Mater. Interfaces XXXX, XXX, XXX–XXX

Scheme 2. Schematics of the Preparation of Photonic Semi-IPN $_{semi}CLC_{solid-PAA-KOH}$, $_{semi}CLC_{solid-PAA-urease}$, and $_{semi}CLC_{solid-PAA-PBA}$ Droplets Compartmentalized in the PAA-Patterned Array Film

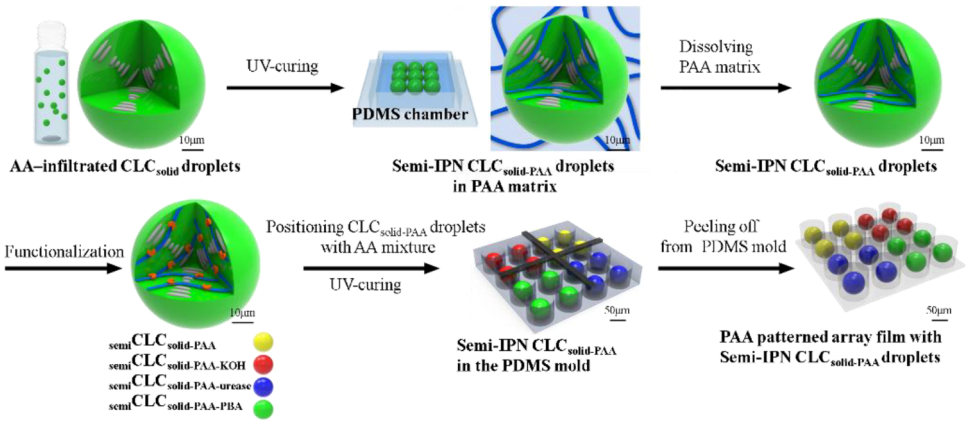

persulfate solution (0.5 g/mL, 5 mL) dropwise. The powders were precipitated by adding ammonium persulfate and centrifuging at 5000 rpm for 15 min using a VS-21SMT centrifuge (Vision, South Korea). The supernatant was decanted, and the powder was dried in a vacuum oven at 40 °C for 1 h. The dried powder was stored for later use. The $CLC_{solid-PAA}$ droplets immobilized with urease (and rho−urease) ($CLC_{solid-PAA-urease}$ (and $CLC_{solid-PAA-rho-urease}$)) in the patterned array films were prepared by the following methods. The patterned array film was immersed in an aqueous EDC/NHS (1/2 v/v, 0.2 M/0.2 M, 1 mL) and left for 2 h. The aqueous urease (and rho−urease) solution (10 mg/mL, 1 mL) was added to the EDC-activated patterned array films in a pH 7 buffer solution, left for 12 h, and then washed with a large amount of water. The patterned array films were tested by immersing them (1 × 1 × 0.1 cm^3) in aqueous analyte solutions (1 mL) of various concentrations.

$CLC_{solid-PAA-PBA}$ Droplets for Glucose Biosensors. PBA immobilization on the photonic IPN $CLC_{solid-PAA}$ droplets was performed using the same method as described above for the urease immobilization process. Here, the CLC_{solid} droplet was prepared with a higher concentration of the chiral dopant (30.5 wt % instead of 29.4 wt %) to ensure a more noticeable color response to the glucose solutions (0.5 mL). An aqueous PBA solution (30 mM, 0.5 mL) was added to the EDC-activated patterned film (1 × 1 × 0.1 cm^3) in a buffer solution (pH 7) and left for 2 h. The resulting PBA-immobilized $CLC_{solid-PAA}$ (abbreviated as $CLC_{solid-PAA-PBA}$) droplets in the patterned film were washed with a large amount of water prior to testing via immersion (1 × 1 × 0.1 cm^3) in an aqueous analyte solution.

$CLC_{solid-PAA-KOH}$ Droplets for Metal Biosensors. The $CLC_{solid-PAA}$ droplets in the PAA patterned array film were treated with K^+ ions by immersing them (1 × 1 × 0.1 cm^3) in an aqueous KOH solution (1 M, 0.5 mL) for 5 min. The resulting KOH-treated $CLC_{solid-PAA}$ (abbreviated as $CLC_{solid-PAA-KOH}$) droplets on the patterned array film were then air-dried. The $CLC_{solid-PAA-KOH}$ droplets on the patterned array film were used for detecting metal ions by immersion (1 × 1 × 0.1 cm^3) in aqueous metal ion solutions (0.5 mL) of various concentrations.

Semi-IPN $_{semi}CLC_{solid-PAA}$ Droplets for Multiple Detections. The CLC_{solid} droplets were functionalized by preparing individually separated semi-IPN $CLC_{solid-PAA}$ droplets (not in the dots of the patterned array film) via the same method as that used for constructing the photonic IPN $CLC_{solid-PAA}$ droplets. To distinguish the semi-IPN ($CLC_{solid-PAA}$) from full-IPN ($CLC_{solid-PAA}$), we denote them as $_{semi}CLC_{solid-PAA}$ and $CLC_{solid-PAA}$, respectively. Here, a linear soluble PAA matrix film was utilized instead of the PAA networks since it was obtained via UV curing of the CLC_{solid} droplets dispersed in the AA monomer without any crosslinkers in the rectangular, unpatterned PDMS mold (Scheme 2). The prepared semi-IPN $CLC_{solid-PAA}$ (abbreviated as $_{semi}CLC_{solid-PAA}$) droplets could be separated from the PAA matrix by dissolving them in a buffer solution (pH 12) and collecting the individually separated $_{semi}CLC_{solid-PAA}$ droplets. Subsequent functionalization of the $_{semi}CLC_{solid-PAA}$ droplets with urease, PBA, and KOH via the aforementioned methods was performed to obtain the corresponding $_{semi}CLC_{solid-PAA-urease}$, $_{semi}CLC_{solid-PAA-PBA}$, and $_{semi}CLC_{solid-PAA-KOH}$ droplets, respectively. The $_{semi}CLC_{solid-PAA-urease}$, $_{semi}CLC_{solid-PAA-PBA}$, and $_{semi}CLC_{solid-PAA-KOH}$ droplets were mixed again with the mixture containing AA monomers (98.5 wt %), TPGDA (0.5 wt %), and Irgacure 500 (1 wt %) and then placed at the desired position in the patterned array film (Scheme 2). The 3 mm thick PDMS film with the adhesive on one side was cut into a "cross" shape and adhered to the PDMS mold as a wall to compartmentalize the $_{semi}CLC_{solid-PAA}$ droplets into four different locations as shown in Figure S6. The PAA-patterned array films containing the photonic $_{semi}CLC_{solid-PAA}$, $_{semi}CLC_{solid-PAA-urease}$, $_{semi}CLC_{solid-PAA-PBA}$, and $_{semi}CLC_{solid-PAA-KOH}$ droplets on four compartmentalized dots were prepared using the abovementioned method so as to construct the PAA-patterned array film containing the photonic IPN $CLC_{solid-PAA}$ droplets in the dots.

Measurements. The reflected colors of the CLC_{solid} and $CLC_{solid-PAA}$ droplets in the patterned array film were observed with an ANA-006 optical microscope (Leitz, Germany) equipped with an STC-TC83USB-AS digital camera (SenTech, Japan) in the reflection mode. The cross-sectional surfaces of the CLC_{solid} and the IPN $CLC_{solid-PAA}$ droplets in the patterned array film were obtained by microtoming (EM UC6, Leica, Austria) epoxy-molded samples using an MC14503 diamond knife (Diatome, Switzerland). The epoxy molding procedure was performed by positioning the CLC_{solid} droplets or the small cut pieces of the patterned array film containing the $CLC_{solid-PAA}$ droplets at the tip of the cap (Cavity Embedding Mold, Ted Pella, USA). Next, the cap was filled with an epoxy mixture of EPON (2 mL), DDSA (1.25 mL), NMA (1.25 mL), and DMP (0.075 mL). Cross-sectional surface images of the CLC_{solid} and $CLC_{solid-PAA}$ droplets were obtained using a model SU8220 field-emission scanning electron microscope (FESEM, Hitachi, Japan) operating at an accelerating voltage of 5 kV. The FESEM samples were prepared by coating the cross-sectional surfaces with platinum. The immobilization of rho−urease in the interior of the photonic IPN $CLC_{solid-PAA-rho-urease}$ droplets was confirmed using the images of the cross-sections obtained using a BX51 fluorescence optical microscope (Olympus, South Korea) at an excitation wavelength of 480 nm. The reflected color was digitalized using CIE XYZ coordinates obtained from the images of the central reflection of the photonic IPN $CLC_{solid-PAA}$ droplets in the patterned array film using Color Grab software (Loomatix, Israel). The xy coordinates from the image were plotted on the xy chromaticity diagram per the CIE 1931 system. The wavelength in the CIE figure ranges from 380 to 700 nm. The dominant wavelength ($\lambda_{dominant}$) was calculated based on the linear line between the chromaticity coordinates of the reference white point (x = 0.3127, y = 0.3290) and the reflected color on the diagram.

https://dx.doi.org/10.1021/acsami.0c15718
ACS Appl. Mater. Interfaces XXXX, XXX, XXX−XXX

Extrapolation to that point on the horseshoe-shaped curve gave the $\lambda_{dominant}$ associated with that point.[34,35]

We tested the influence of the microscope's light intensity and focused on $\lambda_{dominant}$. Figure S7 shows the optical microscopy images and the (x, y) chromaticity diagrams of the photonic $CLC_{solid-PAA}$ droplets at different light intensities and focal planes. The intensity of the microscope was controlled using the dial number in the intensity controller, and the focal plane was adjusted from top to center. All measured $\lambda_{dominant}$ from the (x, y) chromaticity diagrams were 571 nm, indicating that the intensity of light and the focal plane in the microscope has little effect on the measured $\lambda_{dominant}$. The limit of detection (LOD) for the photonic IPN $CLC_{solid-PAA-urease}$ and $CLC_{solid-PAA-KOH}$ droplets was calculated using the following equation: LOD = 3.3 × (SD/s), where SD is the standard deviation obtained from triplicate experiments that were tested with a blank (0 mM) urea solution as the control and s is the corresponding slope of the graph shown in Figures S10 and S12. All experiments were carried out at approximately 25 °C and 50% relative humidity.

RESULTS AND DISCUSSION

Photonic IPN $CLC_{solid-PAA}$ Droplets in the Patterned Array Film. The CLC_{solid} droplets were positioned in the patterned PDMS mold. The PDMS mold has cylindrical array holes in which individual CLC_{solid} droplets can be positioned. The hole diameter of the PDMS mold (110 μm) was close to that of the CLC_{solid} droplet (80 μm). Figure 1a shows the optical microscopy image of the PDMS mold with the AA-infiltrated photonic IPN CLC_{solid} droplets in the holes. Here, the individual CLC_{solid} droplets were separately placed in each hole, and distinct reflection colors were observed from the CLC_{solid} droplets. The PAA-patterned array film was peeled from the PDMS mold after UV curing. Figure 1b exhibits the optical microscopy image of the PAA-patterned array film with the photonic IPN CLC_{solid} droplets in the dots. The photonic IPN $CLC_{solid-PAA}$ droplets were clearly visible, and the blue reflected color of the dry CLC_{solid} droplet became green in the PAA matrix due to PAA infiltration into the empty space of the CLC_{solid} droplets. Thus, the photonic IPN $CLC_{solid-PAA}$ droplets embedded in the PAA patterned array film were successfully produced using the PDMS mold.

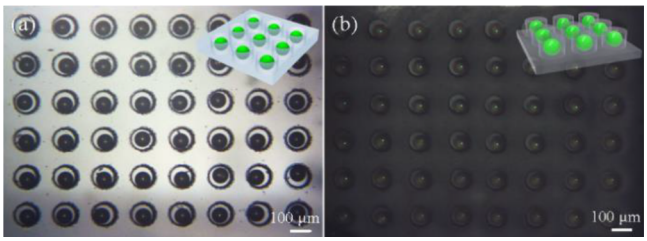

Figure 1. Bright-field optical microscopy images of (a) PDMS mold with AA-infiltrated photonic CLC_{solid} droplets in the holes and (b) PAA-patterned array film containing the photonic IPN $CLC_{solid-PAA}$ droplets in the dots. The insets in (a) and (b) are schematic figures of the PDMS mold with CLC_{solid} droplets in the holes and the patterned array film containing $CLC_{solid-PAA}$ droplets in the dots, respectively.

Figure S4b displays an SEM image of the cross-sectional surface of the photonic IPN $CLC_{solid-PAA}$ droplet. The measured P of the $CLC_{solid-PAA}$ droplets (415 nm) was higher than that of the CLC_{solid} droplets (364 nm) due to the intertwined pH-responsive PAA chains. The measured P of 415 nm had a λ_{PBG} of 540 nm that was calculated using $\lambda_{PBG} = nP$, where n (1.3) was the average reflective index.[13,16] The λ_{PBG} at 540 nm was green and close to the observed color.

pH Responsiveness of the Photonic IPN $CLC_{solid-PAA}$ Droplets. The pH responsiveness of the photonic IPN $CLC_{solid-PAA}$ droplets was tested. Figure 2a shows the optical microscopy images of the photonic IPN $CLC_{solid-PAA}$ droplets in the dots of the PAA-patterned array film at different pH values. Here, the green reflection at pH ≤ 5 transitioned to yellow at pH values of 6 and 7, orange at pH 8, and finally red at pH ≥ 9. In addition to the reflected color change, the PAA matrix surrounding the $CLC_{solid-PAA}$ droplet detached, and a hole in the dot was generated at pH ≥ 5. The hole expanded as the pH levels increased. The overall shape resembled that of frog embryos surrounded by a gelatinous material. The redshift of the reflection color was due to the swelling of the PAA chains caused by the electrostatic repulsion between the anionic carboxylic groups at high pH. The $CLC_{solid-PAA}$ droplet detached from the matrix when the size of the swollen PAA matrix was larger than that of the $CLC_{solid-PAA}$ droplet. Empty spaces were created as a result of the network expansion triggered by the rise in the pH value. The change in the measurable dimensions of the PAA network offered another advantage related to the PAA hydrogel matrix. The reflected color was digitalized using CIE XYZ coordinates derived from images of the central reflection of the photonic IPN $CLC_{solid-PAA}$ droplets in the array film. Figure 2b,c shows the xy chromaticity diagram of the photonic IPN $CLC_{solid-PAA}$ droplets and their $\lambda_{dominant}$ values as a function of pH, respectively.

The $\lambda_{dominant}$ transitioned from green (538 nm) at pH 2 to yellow (571 nm) at pH 7, and finally to red (610 nm) at pH 12. Thus, these calculated $\lambda_{dominant}$ values were in agreement with the colors observed using an optical microscope (Figure 2a). Figure 2d shows the changes in the diameter of the photonic IPN CLC_{solid} droplets in the dots of the PAA-patterned array matrix at various pH values. Here, the diameter increased slightly till pH 5, after which a stepwise increase was noted between pH 6 and 7, and a slight increase was observed at pH ≥ 8. This trend was similar to the changes observed in the reflected color, indicating that the reflected color change was due to the swollen PAA network. The patterned film also possessed many dots on average, as shown in Figure S8; at pH 12 (Figure S8a) and pH 2 (Figure S8b), 25 dots were observed in the optical microscopy images of the 5 × 5 array pattern. The average $\lambda_{dominant}$ and its standard deviation were calculated to be 611 ± 4 and 541 ± 6 nm at pH = 12 and 2, respectively. A small standard deviation (i.e., 4 nm at pH = 12 and 6 nm at pH 2) indicated that the photonic IPN $CLC_{solid-PAA}$ droplets in the dots of the PAA-patterned array matrix were uniform and that the measurement procedure was accurate. Thus, the photonic IPN $CLC_{solid-PAA}$ droplets in the array film were, indeed, pH-sensitive and could be used for constructing pH-responsive biosensors.

We also tested the speed of the pH response with the photonic IPN $CLC_{solid-PAA}$ droplets. Figure S9 shows the optical microscopy images and the measured $\lambda_{dominant}$ of the central reflections of the photonic IPN $CLC_{solid-PAA}$ droplets in the dot of the patterned array film at different elapsed times after pH 12 aqueous buffer solutions were dropped on the dots. The initial green color changed to yellow and then red within 10 min, indicating that the pH response of the photonic IPN $CLC_{solid-PAA}$ droplet is saturated within 10 min and can be measured after that at a steady state. After dropping the solution, we waited for 30 min and then measured the reflected

https://dx.doi.org/10.1021/acsami.0c15718
ACS Appl. Mater. Interfaces XXXX, XXX, XXX−XXX

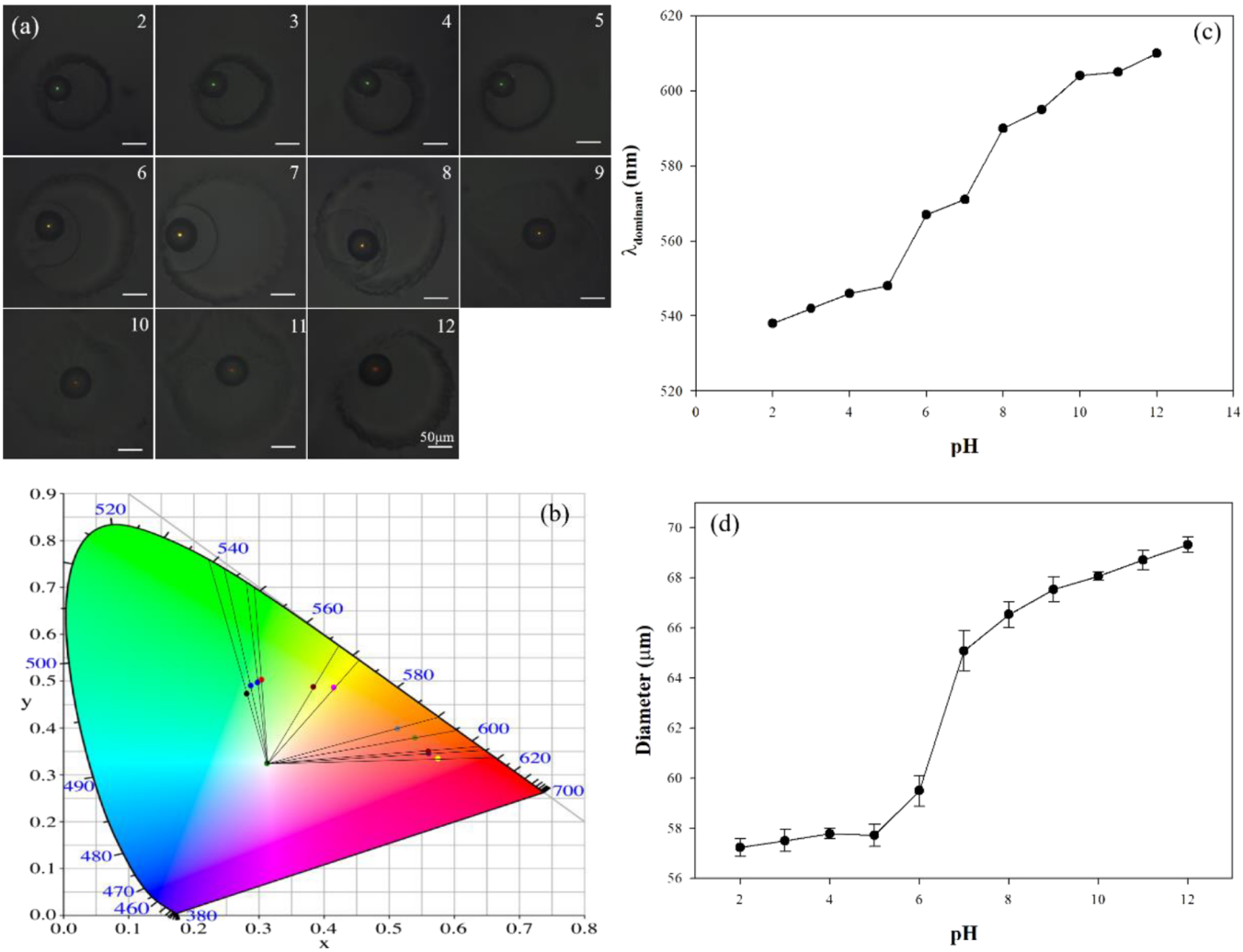

Figure 2. (a) Bright-field optical microscopy images of the photonic IPN $CLC_{solid-PAA}$ droplets in the dot of the patterned array film at various pH levels; numbers represent pH. (b) Corresponding xy chromaticity diagram obtained from the central reflected color in (a). (c) Corresponding $\lambda_{dominant}$ values (measured from (b)) as a function of pH. (d) Diameter of the photonic IPN $CLC_{solid-PAA}$ droplets in the dots of the patterned array film as a function of pH.

color for further experiments, resulting in a longer time than the saturation process.

Enzymatic Urea Biosensor Application. Urea is an important biomarker for the diagnosis of kidney and liver diseases. The photonic IPN $CLC_{solid-PAA}$ droplet in the patterned array film developed in this study was used for a urea biosensor application via the immobilization of urease. The immobilization of urease was confirmed with fluorescent rho−urease, which can be observed through fluorescent microscopy. Figure 3a,b shows the fluorescence microscopy images of the photonic IPN $CLC_{solid-PAA}$ droplets in the patterned array film before and after the immobilization of rho−urease, respectively.

Before immobilization (Figure 3a), the photonic IPN $CLC_{solid-PAA}$ droplet showed a blue fluorescent color, which is from the CLC_{solid} droplet without immobilization. However, the immobilization of rho−urease resulted in a color change to yellow (Figure 3b) with a similarly colored yellow background. The yellow fluorescence observed was because of the high concentration of rhodamine 6G in the system.[34] The yellow background was transitioned to green after all unreacted rhodamine 6G molecules were removed and the photonic IPN

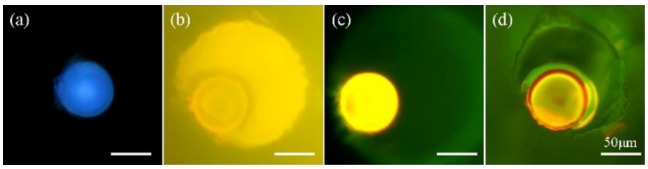

Figure 3. Florescence microscopy images of the photonic IPN $CLC_{solid-PAA}$ droplets in the PAA-patterned array film at pH 7 (a) without and (b, c) with rho−urease immobilization, (b) before and (c) after removal of the unreacted rhodamine 6G. (d) Cross-section of the epoxy-molded photonic IPN $CLC_{solid-PAA-rho-urease}$ droplets in the patterned array film.

$CLC_{solid-PAA}$ droplet remained yellow (Figure 3c). These observations served as a confirmation of the immobilization process on the photonic IPN $CLC_{solid-PAA}$ droplets.

The immobilization of rho−urease in the interior of the photonic IPN $CLC_{solid-PAA}$ droplet was confirmed by examining the cross-sections of the photonic IPN $CLC_{solid-PAA-rho-urease}$ droplets, as shown in Figure 3d. As noted, the entire cross-sectioned area was yellow even though the yellow color noted at the periphery was more intense than

https://dx.doi.org/10.1021/acsami.0c15718
ACS Appl. Mater. Interfaces XXXX, XXX, XXX−XXX

that seen in the droplet's interior. This indicated that even though urease molecules had penetrated the periphery and were immobilized in the interior of the IPN CLC_{solid} droplet, noticeably more urease molecules were immobilized at the external surface. The reaction between urease and urea could therefore occur inside the IPN CLC_{solid} droplet and induce changes in the reflected color.

The photonic IPN $CLC_{solid-PAA-urease}$ droplets in the patterned array film were tested to determine their ability to detect urea. Figure 4a shows the optical microscopy images of the photonic IPN $CLC_{solid-PAA-urease}$ droplets in the dots after treatment with aqueous urea solutions at various concentrations (C_{urea}). The initial green color observed at C_{urea} = 0 and 3.5 mM (Figure 4 a(i-ii)) transitioned to yellow at C_{urea} = 5 mM (Figure 4a(iii)), orange at C_{urea} = 6.5 and 7.5 mM (Figure 4a(iv–v)), and finally to red at $C_{urea} \geq 14$ mM (Figure 4a(vi–viii)).

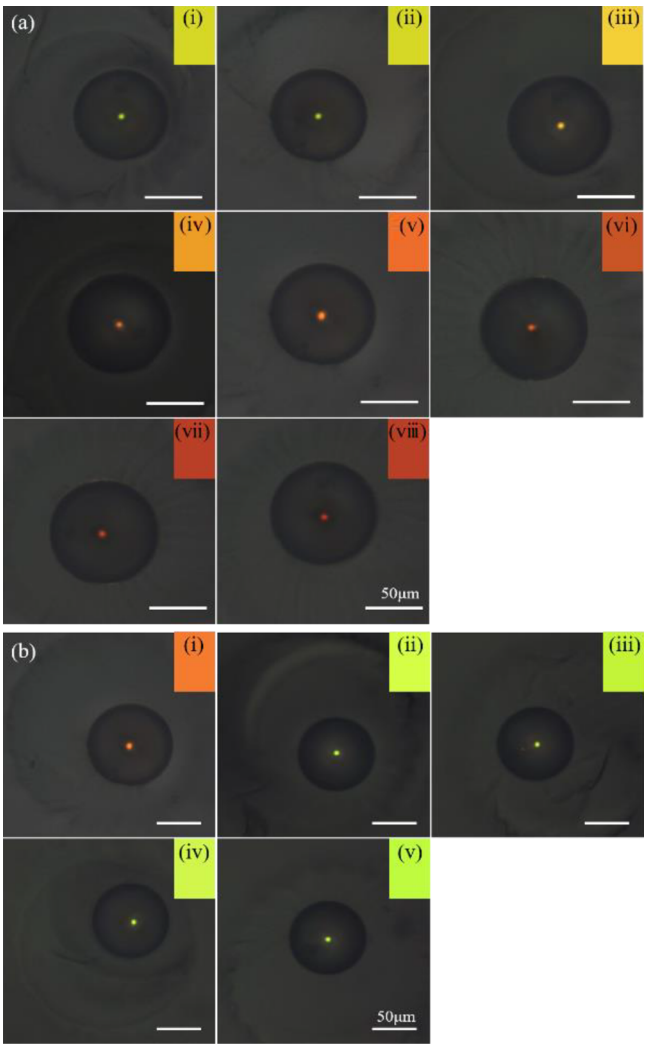

Figure 4. Bright-field optical microscopy images of photonic IPN $CLC_{solid-PAA-urease}$ droplets in patterned array films treated with (a) aqueous urea solutions (0.5 mL) at C_{urea} = (i) 0 (DI water), (ii) 3.5, (iii) 5, (iv) 6.5, (v) 7.5, (vi) 14, (vii) 60, and (viii) 120 mM and (b) other aqueous solutions (0.5 mL), namely, (i) urea (7.5 mM), (ii) glucose (10 mM), (iii) cholesterol (6.5 mM), (iv) ascorbic acid (1.5 mM), and (v) uric acid (0.4 mM). Insets represent the observed colors of the central reflections of the $CLC_{solid-PAA}$ droplets.

The photonic IPN $CLC_{solid-PAA-urease}$ droplets in the patterned array film were tested to determine their ability to detect urea. Figure 4a shows the optical microscopy images of the photonic IPN $CLC_{solid-PAA-urease}$ droplets in the dots after treatment with aqueous urea solutions of various concentrations (C_{urea}). The initial green color observed at C_{urea} = 0 and 3.5 mM (Figure 4a(i,ii)) transitioned to yellow at C_{urea} = 5 mM (Figure 4a(iii)), orange at C_{urea} = 6.5 and 7.5 mM (Figure 4a(iv,v)), and finally to red at $C_{urea} \geq 14$ mM (Figure 4a(vi–viii)). Figure S10a,b shows the corresponding XY chromaticity diagrams obtained for the reflected central color in Figure 4a and the plot of $\lambda_{dominant}$ as a function of C_{urea}, respectively. The color associated with the respective $\lambda_{dominant}$ values transitioned from green (567 nm) at C_{urea} = 0 and 3.5 mM to yellow (576 nm) at C_{urea} = 5 mM, and finally to red (593 nm) at C_{urea} = 14 mM. The color of the central reflection of the photonic IPN $CLC_{solid-PAA}$ droplets in the patterned array film exhibited similar responses to changes in the pH of the system (Figure 2), and the calculated $\lambda_{dominant}$ values were in good agreement with the colors observed during optical microscopy (Figure 4a). The abnormal concentration of urea extracted from the human blood sample was over 7.5 mM; thus, a transition to red could be used as an "alarm signal" for uremia. Although the primary mode of excretion is in the urine via the kidneys, urea is also secreted in bodily fluids, such as sweat, blood, and saliva.[36] Because urea is an important biomarker for diagnosing kidney and liver issues,[37] elevated levels in human blood are symptomatic of chronic kidney and renal diseases. This condition is referred to as "uremia." The normal range of urea in human serum is from 2.6 to 6.5 mM;[38] 7.5 mM is higher than that. The linear range and LOD of the photonic IPN $CLC_{solid-PAA-urease}$ droplet in the patterned array film were calculated from the plots of the $\lambda_{dominant}$ versus C_{urea} (Figure S10b). The linear range and LOD were 0–7.5 mM and 0.027 mM, respectively. These are good enough to measure urea in human serum.

The selectivity of the photonic IPN $CLC_{solid-PAA-urease}$ droplets in the patterned array film was also tested using a variety of aqueous solutions (0.5 mL), including urea (7.5 mM), glucose (10 mM), cholesterol (6.5 mM), ascorbic acid (1.5 mM), and uric acid (0.4 mM) all of which are the main components of human blood. The concentration of the solution was maintained slightly above the normal concentration range found in the human blood.[18,19,27] Figure 4b shows the optical microscopy images of the photonic IPN $CLC_{solid-urease}$ droplets in the patterned array film treated with these aqueous solutions. The measured $\lambda_{dominant}$ are 591.0 ± 1.6, 565.8 ± 2.0, 565.6 ± 2.1, 566.4 ± 2.2, and 566.2 ± 1.6 nm for urea, glucose, cholesterol, ascorbic acid, and uric acid, respectively.

Except for urea, the initial green color remained unchanged, indicating that the droplets were extremely selective, and thus, could serve as an enzyme-based urea biosensor.

Nonenzymatic Glucose Biosensor. The photonic IPN $CLC_{solid-PAA-PBA}$ droplets in the dots of the patterned array films were tested for glucose detection purposes. Figure 5a shows the optical microscopy images of the droplets in the patterned array film when treated with aqueous glucose solutions of various concentrations (C_g). The initial mint color at C_g = 0 and 2 mM (Figure 5a(i,ii)) transitioned to green at C_g = 5 mM (Figure 5a(iii)), yellow at C_g = 10 mM (Figure 5a(iv)), orange at C_g = 15 mM (Figure 5a(v)), and finally to orange/red at C_g = 20 mM (Figure 5a(vi)). The

https://dx.doi.org/10.1021/acsami.0c15718
ACS Appl. Mater. Interfaces XXXX, XXX, XXX–XXX

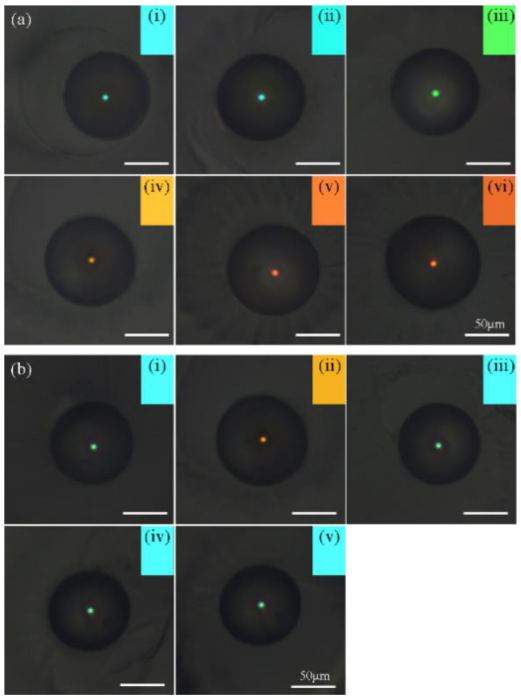

Figure 5. Bright-field optical microscopy images of photonic IPN $CLC_{solid-PAA-PBA}$ droplets in patterned array films treated with (a) aqueous glucose solutions (0.5 mL) at C_g = (i) 0 (DI water), (ii) 2, (iii) 5, (iv) 10, (v) 15, and (vi) 20 mM, and (b) other aqueous solutions (0.5 mL) of (i) urea (7.5 mM), (ii) glucose (10 mM), (iii) cholesterol (6.5 mM), (iv) ascorbic acid (1.5 mM), and (v) uric acid (0.4 mM). Insets represent the observed colors of the central reflections of the $CLC_{solid-PAA-PBA}$ droplets.

abnormally high glucose concentration in the human blood sample, which was taken from a diabetic patient, was over 11 mM; the noticeable orange/red color change thus could be used as an "alarm signal" for diabetes. Figure S11a,b shows the xy chromaticity diagram obtained from the respective reflected central color seen in Figure 5a and the plot of $\lambda_{dominant}$ was determined as a function of C_g, respectively. The calculated $\lambda_{dominant}$ values were in agreement with the colors observed during optical microscopy (Figure 5a).

The selectivity of the photonic IPN $CLC_{solid-PAA-PBA}$ droplets in the patterned array films was also tested using other aqueous solutions, namely, urea (7.5 mM), glucose (10 mM), cholesterol (6.5 mM), ascorbic acid (1.5 mM), and uric acid (0.4 mM). The concentration of the aqueous solution was maintained slightly higher than the normal concentration range found in the human blood as mentioned in the urea test. The normal blood glucose level (tested while fasting) for patients without diabetes is between 3.9 and 7.1 mM (70−130 mg/dL).[39] 10 mM of glucose concentration is higher than that. Figure 5b shows the optical microscopy images of the photonic IPN $CLC_{solid-PAA-PBA}$ droplets in the patterned array films treated with these aqueous solutions. The measured $\lambda_{dominant}$ are 493.0 ± 1.6, 579.8 ± 2.2, 493.4 ± 1.5, 492.8 ± 1.5, and 492.4 ± 1.7 nm for urea, glucose, cholesterol, ascorbic acid, and uric acid, respectively. Except for the glucose sample, the initial green reflected color remained unchanged, indicating that the photonic IPN $CLC_{solid-PAA-PBA}$ droplets were highly selective, and thus, could be used as a nonenzymatic glucose biosensor.

Metal Ion Detection Using Photonic IPN $CLC_{solid-PAA-KOH}$ Droplets. The photonic IPN $CLC_{solid-PAA-KOH}$ droplets in the dot array were applied for metal ion detection purposes. Briefly, a 1 M KOH aqueous solution was treated to form COO^-K^+ salts known to inhibit hydrogen bonding between the carboxylic groups, expand the intertwined PAA network, increase the photonic helicoidal pitch, and redshift the reflected color. The prepared photonic IPN $CLC_{solid-PAA-KOH}$ droplets exhibited a red reflected color in water, as shown in Figure 6a(i). The Ca^{2+} ion was first

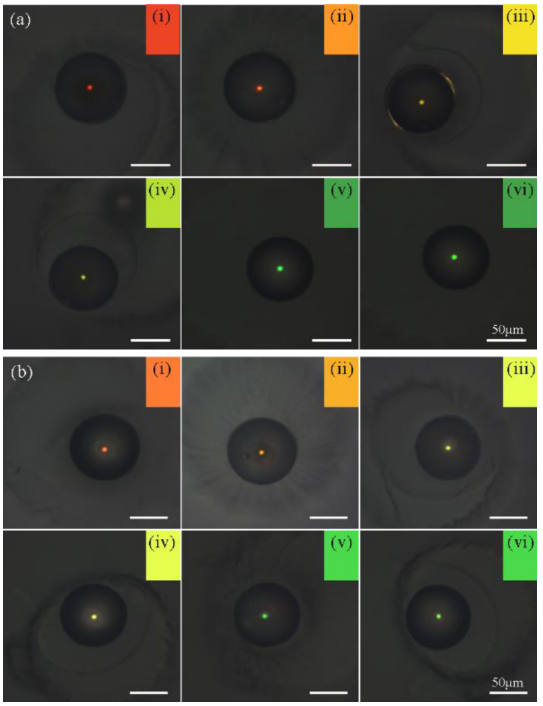

Figure 6. Bright-field optical microscopy images of photonic IPN $CLC_{solid-PAA-KOH}$ droplets in the patterned array films treated with (a) aqueous $CaCl_2$ solutions (0.5 mL) at C_{ca} = (i) 0 (DI water), (ii) 0.1, (iii) 0.2, (iv) 0.3, (v) 0.4, and (vi) 0.8 mM and (b) other aqueous metal ion solutions (0.5 mL), namely, (i) $NaNO_3$ (0.8 mM), (ii) $Cu(NO_3)_2$ (0.4 mM), (iii) $Zn(NO_3)_2$ (0.4 mM), (iv) $FeCl_2$ (0.4 mM), (v) $Mg(NO_3)_2$ (0.4 mM), and (vi) $CaCl_2$ (0.4 mM). Insets represent the observed colors of the central reflections of the $CLC_{solid-PAA-KOH}$ droplets.

tested among the divalent ions as a model study because it exists in the largest amount in human blood.[40] Because a divalent metal ion of Ca^{2+} could form a −COO−Ca−OOC− bond, the degree of the swelling of the photonic IPN $CLC_{solid-PAA-KOH}$ droplets could be reduced after treatment with an aqueous calcium ion solution. Figure 6a(ii−vi) shows the optical microscopy images of photonic IPN $CLC_{solid-PAA-KOH}$ droplets in patterned array films treated with aqueous $CaCl_2$ solutions of different C_{ca}. The initial red reflected color (Figure 6a(i)) was blueshifted to orange at C_{ca} = 0.1 mM (Figure 6a(ii)), yellow at C_{ca} = 0.2 mM (Figure 6a(iii)), lime/green at C_{ca} = 0.3 mM (Figure 6a(iv)), and finally to green at $C_{ca} \geq 0.4$ mM (Figure 6a(v−vi)), indicating that the −COO−Ca−OOC− bond was formed in the PAA network after treatment with the aqueous calcium ion solution. The degree of the deswelling (i.e., the extent of blueshifting) increased as C_{ca} was increased. Thus, the photonic IPN $CLC_{solid-PAA-KOH}$ droplets in the patterned array film could be

https://dx.doi.org/10.1021/acsami.0c15718
ACS Appl. Mater. Interfaces XXXX, XXX, XXX−XXX

used for detecting divalent metal ions. Similar to the photonic IPN $CLC_{solid-PAA-urease}$ and $CLC_{solid-PAA-PBA}$ droplets in the patterned array films mentioned earlier, the measured $\lambda_{dominant}$ values from the xy chromaticity diagram obtained from the central reflected color (in Figure 6a) were in agreement with the color observed during optical microscopy, as shown in Figure S12a,b.

The linear range and LOD of the photonic $CLC_{solid-PAA-KOH}$ droplet in the patterned array film were calculated from the plots of the $\lambda_{dominant}$ versus C_{ca} (Figure S12b). The linear range and LOD were 0−0.4 mM and 9 μM, respectively.

The formation of the bridging structure with the divalent ions was subsequently evaluated using other metal ions. Figure 6b shows the optical microscopy images of $CLC_{solid-PAA-KOH}$ droplets in the patterned array film after the addition of aqueous metal solutions (0.5 mL), namely, $NaNO_3$ (0.8 mM), $Cu(NO_3)_2$ (0.4 mM), $Zn(NO_3)_2$ (0.4 mM), $FeCl_2$ (0.4 mM), $Mg(NO_3)_2$ (0.4 mM), and $CaCl_2$ (0.4 mM). The concentrations of the divalent ions were maintained at 0.4 mM because the photonic IPN $CLC_{solid-PAA-KOH}$ droplets changed the reflected color completely at C_{ca} = 0.4 mM, as shown in Figure 6. Other metal ions were maintained at the same concentration to compare the detection ability among divalent ions. Taking into account the valence of the ion, the concentration of Na^+ was twice that of the divalent ions. The addition of monovalent Na^+ ions produced little change to the red reflected color of the $CLC_{solid-IPN-KOH}$ droplet because the monovalent ions were unable to form the bridging structure (Figure 6b(i)). However, treatment with divalent ions such as Cu^{2+}, Zn^{2+}, Fe^{2+}, Mg^{2+}, and Ca^{2+} resulted in a color transition from orange/yellow (Cu^{2+}, Figure 6b(ii)), lime (Zn^{2+}, Figure 6b(iii)), lime/green (Fe^{2+}, Figure 6b(iv)), and finally to green (Mg^{2+} and Ca^{2+}, Figure 6b(v,vi)), respectively. The reflected colors of the photonic IPN $CLC_{solid-PAA-KOH}$ droplets in response to 0.4 mM of Mg^{2+} and Ca^{2+} ions are similar to each other. However, the measured $\lambda_{dominant}$ values were 555 and 548 nm for Mg^{2+} and Ca^{2+}, respectively, revealing that Ca^{2+} is more blueshifted than Mg^{2+}. Most of the divalent metal ions were able to form the bridging structure, thereby preventing the swelling of the $CLC_{solid-PAA-KOH}$ droplets and leading to a blueshift in the reflected color. Figure S13a,b shows the corresponding xy chromaticity diagrams obtained from the reflected central color seen in Figure 6b, and the plot of the $\lambda_{dominant}$ values with various divalent metal ions, respectively. The $\lambda_{dominant}$ values were 582, 573, 568, 555, and 548 nm for Cu^{2+}, Zn^{2+}, Fe^{2+}, Mg^{2+}, and Ca^{2+}, respectively.

The magnitude of the blueshift followed the order of Cu^{2+} < Zn^{2+} < Fe^{2+} < Mg^{2+} < Ca^{2+}, which was consistent with previously reported data.[28,41,42] Thus, the $CLC_{solid-PAA-KOH}$ droplets can detect any divalent ions without selectivity; although, Ca^{2+} and Mg^{2+} have the highest interaction between the carboxylic group and divalent metal ions.[40] The main divalent metal ions in human serum are Ca^{2+} and Mg^{2+}, and other metal ions exist in an extremely small amount so that they cannot be detected with our developed photonic sensor.[40] Although the photonic $CLC_{solid-IPN-KOH}$ balls are not specific to the type of divalent metal ions, the changing of the color of the photonic $CLC_{solid-IPN-KOH}$ balls indicates the abnormally high amounts of the combined Mg^{2+} and Ca^{2+} ions.

A metal ion cannot have the same tendency to complex with carboxylic acids even though it has an equivalent valency. It depends on several factors. Ederth and Claesson explained that the amount of adsorption of divalent ions on the carboxylic acid surface could be rationalized in terms of hydration of the cations.[43] Because Mg^{2+} is smaller than Ca^{2+}, it is more strongly hydrated, and hydration provides an energy barrier against adsorption. To obtain more meaningful knowledge regarding the binding capability of divalent ions, Bala conducted first-principles calculations based on density functional theory to study the interaction of different cations with the simplest carboxylic acid and acetic acid.[30] They also found that Ca^{+2} has the highest binding strength toward carboxylic acid. However, it is quite complex to explain clearly the order of the binding strength between carboxylic groups and divalent metal ions, which is out of the scope of the current study.

The reusability of the $CLC_{solid-PAA-KOH}$ droplets in the patterned array films, which was already tested using various aqueous $CaCl_2$ solutions, was evaluated following a HNO_3 treatment through which −COOH could be recovered from the −COO−Ca−COO− structure. Figure 7 shows the optical microscopy images of the $CLC_{solid-PAA-KOH}$ droplets in the patterned array films after sequential KOH (1 M), $CaCl_2$ (0.3 mM), and HNO_3 (0.1 M) aqueous solution (0.5 mL) treatments over four cycles. The concentration of 0.3 mM for the $CaCl_2$ aqueous solution was chosen because it changed to distinct yellow, as shown in Figure 6a, and the concentrations of 1 M for KOH and 0.1 M for HNO_3 aqueous solutions were strong enough to make and dismantle complexes between the carboxylic acid and metal ion, respectively. Red, yellow, and green reflections were observed after sequential KOH, $CaCl_2$, and HNO_3 treatments (Figure 7a−c) during the first cycle. The yellow reflection color after

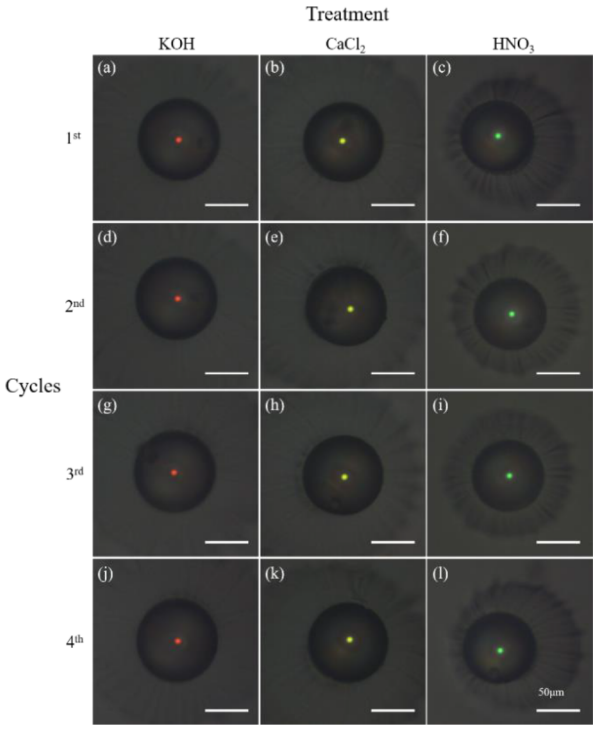

Figure 7. Bright-field optical microscopy images of the $CLC_{solid-PAA-KOH}$ droplets in the patterned array films after (a, d, g, j) KOH (1 M, 0.5 mL), (b, e, h, k) $CaCl_2$ (0.3 mM, 0.5 mL), and (c, f, i, l) HNO_3 (0.1 M, 0.5 mL) treatments over four cycles of (a−c), (d−f), (g−i), and (j−l). The scale bar represents 50 μm in all images.

https://dx.doi.org/10.1021/acsami.0c15718
ACS Appl. Mater. Interfaces XXXX, XXX, XXX−XXX

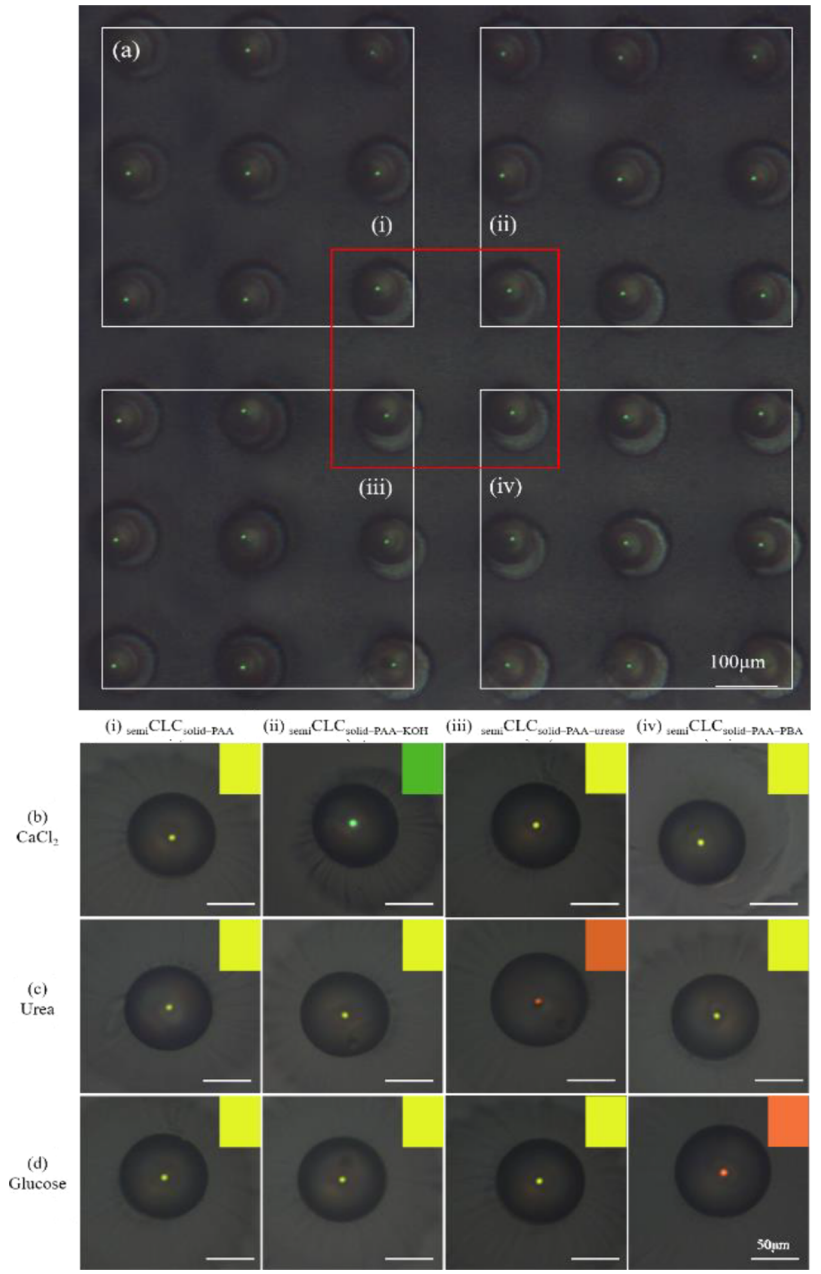

Figure 8. (a) Bright-field optical microscopy images of 6 × 6 patterned array films containing (i) $_{semi}CLC_{solid-PAA}$, (ii) $_{semi}CLC_{solid-PAA-KOH}$, (iii) $_{semi}CLC_{solid-PAA-urease}$, and (iv) $_{semi}CLC_{solid-PAA-PBA}$ droplets compartmentalized in the upper left, upper right, lower left, and lower right sections, respectively; white boxes represent the compartmentalized sections. (b–d) The enlarged bright-field optical microscopy images of the dots of the four sections of the center of the 2 × 2 patterned array film (red-boxed region in (a)) containing (i) $CLC_{solid-PAA}$, (ii) $CLC_{solid-PAA-KOH}$, (iii) $CLC_{solid-PAA-urease}$, and (iv) $CLC_{solid-PAA-PBA}$ droplets compartmentalized in the upper left, upper right, lower left, and lower right sections, respectively, after (b) $CaCl_2$ (0.4 mM), (c) urea (14 mM), and (d) glucose (15 mM) aqueous solution (0.5 mL) treatments. All CLC_{solid} droplets were prepared at ϕ = 29.4 wt %.

$CaCl_2$ treatment (Figure 7b) became green after HNO_3 treatment (Figure 7c) via the formation of −COOH from the −COO−Ca−COO− structure. The red, yellow, and green reflection colors were completely recovered after undergoing the same sequential treatments using KOH, $CaCl_2$, and HNO_3 during the second and third cycles (Figure 7d–i). The measured $\lambda_{dominant}$ values after KOH treatment are 603 nm (Figure 7a), 602 nm (Figure 7d), 602 nm (Figure 7g), and 604 nm (Figure 7j) for the first, second, third, and fourth treatments, respectively.

This finding indicated that the Ca^{2+}-treated $CLC_{solid-PAA-KOH}$ droplets in the patterned array films could be made reusable via the HNO_3 treatment. Because this alternation between green and red was observed until the end of the fourth cycle (Figure 7j–l), further tests were not conducted.

Multiple Detections Using Semi-IPN $_{semi}CLC_{solid-PAA}$ Droplets. The individually separated $_{semi}CLC_{solid-PAA}$ droplets were first tested for their pH responsiveness, as shown in Figure S14. The results obtained were similar to the results noted for the photonic IPN $CLC_{solid-PAA}$ droplets in the dots

https://dx.doi.org/10.1021/acsami.0c15718
ACS Appl. Mater. Interfaces XXXX, XXX, XXX−XXX

of the patterned array films at various pH levels (Figure 2a), indicating that the linear PAA chains were intertwined in the space of the CLC_{solid} droplets that had been created via the extraction of the chiral dopant. The functionalized $_{semi}CLC_{solid-PAA-KOH}$, $_{semi}CLC_{solid-PAA-urease}$, and $_{semi}CLC_{solid-PAA-PBA}$ droplets were used for multiple detections as model studies. The patterned array film was employed for multiple detections by first compartmentalizing the CLC_{solid} droplets in the desired positions in the patterned array films. The compartmentalization of the CLC_{solid} droplets in the four different locations mentioned earlier was demonstrated by positioning the CLC_{solid} droplets with orange/red, yellow/green, green, and green/blue central color transitions (prepared at ϕ = 24.0, 29.4, 31.5, and 33.0 wt %, respectively) in different compartments of the O_2 plasma-treated PDMS mold, as shown in Figure S15. The CLC_{solid} droplets at different ϕ values could be compartmentalized in each section, indicating that the CLC_{solid} droplets can be used for multiple detections if the functionalized $CLC_{solid-PAA}$ droplets were used. The individually separated $_{semi}CLC_{solid-PAA}$ could be functionalized and compartmentalized for multiple detections.

Figure 8a shows the photographs of 6 × 6 patterned array films which contain $_{semi}CLC_{solid-PAA}$, $_{semi}CLC_{solid-PAA-KOH}$, $_{semi}CLC_{solid-PAA-urease}$, and $_{semi}CLC_{solid-PAA-PBA}$ droplets in the upper left, upper right, lower left, and lower right sections, respectively. All $_{semi}CLC_{solid-PAA}$ droplets were prepared at ϕ = 29.4 wt %. Figure 8b–d shows the optical microscopy images of the enlarged individual dots of the four sections (red boxed region in Figure 8a) after $CaCl_2$ (0.4 mM), urea (14 mM), and glucose (15 mM) aqueous solution treatments. The concentrations of $CaCl_2$, urea, and aqueous glucose solutions were chosen because the reflected colors at those concentrations were completely changed from the separate experiments shown in Figures 4–6. A response was noted for the $_{semi}CLC_{solid-PAA-KOH}$ (Figure 8(ii)), $_{semi}CLC_{solid-PAA-urease}$ (Figure 8(iii)), and $_{semi}CLC_{solid-PAA-PBA}$ (Figure 8(iv)) droplets to the $CaCl_2$, urea, and glucose only aqueous solutions, respectively, whereas the $_{semi}CLC_{solid-PAA}$ (Figure 8(i)) droplets were unresponsive to any treatments. These findings indicate that the $_{semi}CLC_{solid-PAA-KOH}$, $_{semi}CLC_{solid-PAA-urease}$, and $_{semi}CLC_{solid-PAA-PBA}$ droplets were highly selective for divalent metal ions, urea, and glucose, respectively, and that multiple detections were possible in one patterned array film. The same tests were performed with human serum as shown in Figure S16 in which the aqueous test sample was made with (10 ×) diluted human serum with DI water instead of pure DI water. Similar results were obtained, indicating that the photonic IPN CLC_{solid} droplets can be used with human blood samples. The selectivity of the mixture solutions was also tested. Figure S17 shows the optical microscopy images of the individual dots of the four sections after $CaCl_2$ (0.4 mM) + urea (14 mM), $CaCl_2$ (0.4 mM) + glucose (15 mM), urea (14 mM) + glucose (15 mM), and $CaCl_2$ (0.4 mM) + urea (14 mM) + glucose (15 mM) aqueous solution (0.5 mL) treatments. Similar to the results from Figure 8b, the $CaCl_2$/urea, $CaCl_2$/glucose, urea/glucose, and $CaCl_2$/urea/glucose aqueous solutions responded to the $_{semi}CLC_{solid-PAA-KOH}$/$_{semi}CLC_{solid-PAA-urease}$, $_{semi}CLC_{solid-PAA-KOH}$/$_{semi}CLC_{solid-PAA-PBA}$, $_{semi}CLC_{solid-PAA-urease}$/$_{semi}CLC_{solid-PAA-PBA}$, $_{semi}CLC_{solid-PAA-KOH}$/$_{semi}CLC_{solid-PAA-urease}$/$_{semi}CLC_{solid-PAA-PBA}$ droplets, respectively. In this study, we successfully demonstrated that multiple detections were possible with PAA-patterned array films via the compartmentalized $_{semi}CLC_{solid-PAA}$ droplets in the dots, facilitating various sensors with different receptors or treatments.

CONCLUSIONS

The photonic CLC_{solid} droplets could be used as individual small sensors in the dots of patterned array films. The photonic CLC_{solid} droplets were used as full- and semi-IPN structures with intertwined PAA networks in the patterned array films. The photonic full-IPN CLC_{solid} droplets in the patterned array films were generated when the photonic CLC_{solid} droplets located in the holes of the PDMS mold were subjected to UV curing using a cross-linkable AA mixture, peeled from the PDMS mold, functionalized with receptors, and then used as patch-type patterned sensors that possessed numerous small analytical spherical photonic sensors in the dots.

The semi-IPN structures in photonic CLC_{solid} droplets and their application in multiple sensors were examined using photonic CLC_{solid} droplets UV-cured with AA monomers without the crosslinker. Separation from the PAA matrix, functionalization using different receptors, compartmentalization in various locations of the dots, and UV-curing with a cross-linkable AA mixture all served to generate patterned array films. The photonic IPN $CLC_{solid-PAA}$ droplets in the patterned array films were successfully applied for the detection of divalent metal ions, urea, and glucose via the treatment of KOH, the immobilization of urease, and the reaction with the nonenzyme PBA, respectively. This resulted in a single-analyte sensor with a full-IPN structure, and a multiple-analyte sensor was developed using the semi-IPN structure. The resulting sensors were extremely selective to the major components in human serum and exhibited relatively good sensitivity to the stability of the components facilitated via solid-state structures. These new platform-type patterned array films impregnated with photonic IPN CLC_{solid} droplets resulted in higher accuracy in the averaged data and multiple detections using various analytical dots, thereby opening the door for many exciting applications with various combinations of responsive hydrogel matrixes and receptors.

ASSOCIATED CONTENT

Supporting Information

The Supporting Information is available free of charge at https://pubs.acs.org/doi/10.1021/acsami.0c15718.

Experimental setup for the production of CLC_{solid} droplets using microfluidics, omnidirectional UV curing machine, PDMS mold for droplet array, and PDMS-based microfluidic device for analyte testing, SEM results of the cross-sectional surface of the photonic CLC_{solid} droplets, photographic images of patterned silicon wafer and PDMS mold peeled off from the patterned silicon wafer, bright-field optical microscopy images of the patterned array film compartmentalized into four different locations, xy chromaticity diagrams of the photonic IPN $CLC_{solid-PAA}$, $CLC_{solid-PAA-urease}$, $CLC_{solid-PAA-PBA}$, and $CLC_{solid-PAA-KOH}$ droplets and optical microscopy images of the photonic IPN $CLC_{solid-PAA}$, $CLC_{solid-PAA-urease}$, $CLC_{solid-PAA-PBA}$, and $CLC_{solid-PAA-KOH}$ droplets under different conditions, bright-field optical microscopy images of the photonic $_{semi}CLC_{solid-PAA}$ droplets and PDMS mold with CLC_{solid} droplets prepared at different ϕ values (PDF)

https://dx.doi.org/10.1021/acsami.0c15718
ACS Appl. Mater. Interfaces XXXX, XXX, XXX–XXX

AUTHOR INFORMATION

Corresponding Author

Soo-Young Park − *School of Applied Chemical Engineering, Polymeric Nano Materials Laboratory, Kyungpook National University, Daegu 41566, Republic of Korea;* orcid.org/0000-0001-6796-4929; Email: psy@knu.ac.kr

Author

Ye-Ji Kim − *School of Applied Chemical Engineering, Polymeric Nano Materials Laboratory, Kyungpook National University, Daegu 41566, Republic of Korea*

Complete contact information is available at: https://pubs.acs.org/10.1021/acsami.0c15718

Author Contributions

Y.-J.K. conducted all related experiments and S.-Y.P. supervised these works and wrote the manuscript.

Notes

The authors declare no competing financial interest.

ACKNOWLEDGMENTS

This work was supported by the National Research Foundation of Korea (2020R1A2B5B02001556).

ABBREVIATIONS

CLC_{solid}, solid-state cholesteric liquid crystal
CB15, (*S*)-4-cyano-4′-(2-methylbutyl)biphenyl
DDSA, dodecenylsuccinic anhydride
DI, deionized water
DMP, 2,4,6-tris(dimethylaminomethyl)phenol
EDC•HCl, *N*-(3-dimethylaminopropyl)-*N*′-ethylcarbodiimide hydrochloride
EPON, Poly/Bed® 812
FESEM, field-emission scanning electron microscopy
IPN, interpenetrating polymer network
NHS, *N*-hydroxysuccinimide
NMA, nadic methyl anhydride
PAA, poly(acrylic acid)
PBA, phenylboronic acid
PBG, photonic bandgap
PDMS, polydimethylsiloxane
PFOTS, trichloro(1H,1H,2H,2H-perfluorooctyl)silane
PVA, poly(vinyl alcohol)
SEM, scanning electron microscopy
TEOS, tetraethyl orthosilicate
TPGDA, tripropylene glycol diacrylate.

REFERENCES

(1) Lin, S.-Y.; Fleming, J. G.; Chow, E. Two-and Three-dimensional Photonic Crystals Built with VLSI tools. *MRS Bull.* **2001**, *26*, 627−631.
(2) Turberfield, A. Photonic Crystals Made by Holographic Lithography. *MRS Bull.* **2001**, *26*, 632−636.
(3) Hung, J.; Gao, W.; Tam, W. Y. Optical Activities of Micro-spiral Photonic Crystals Fabricated by Multi-beam Holographic Lithography. *J. Opt.* **2011**, *13*, 095102−095111.
(4) Kondo, T.; Matsuo, S.; Juodkazis, S.; Misawa, H. Femtosecond Laser Interference Technique with Diffractive Beam Splitter for Fabrication of Three-dimensional Photonic Crystals. *Appl. Phys. Lett.* **2001**, *79*, 725−727.
(5) Wijnhoven, J. E. G. J.; Vos, W. L. Preparation of Photonic Crystals Made of Air Spheres in Titania. *Science* **1998**, *281*, 802−804.
(6) Subramania, G.; Biswas, R.; Constant, K.; Sigalas, M. M.; Ho, K. M. Structural Characterization of Thin Film Photonic Crystals. *Phys. Rev. B* **2001**, *63*, 235111−235118.
(7) Park, S. H.; Xia, Y. Assembly of Mesoscale Particles Over Large Areas and its Application in Fabricating Tunable Optical Filters. *Langmuir* **1999**, *15*, 266−273.
(8) Wang, M.; Zou, C.; Sun, J.; Zhang, L.; Wang, L.; Xiao, J.; Li, F.; Song, P.; Yang, H. Asymmetric Tunable Photonic Bandgaps in Self-organized 3D Nanostructure of Polymer-stabilized Blue Phase I Modulated by Voltage Polarity. *Adv. Funct. Mater.* **2017**, *27*, 1702261−1702269.
(9) Sveinbjornsson, B. R.; Weitekamp, R. A.; Miyake, G. M.; Xia, Y.; Atwater, H. A.; Grubbs, R. H. Rapid Self-Assembly of Brush Block Copolymers to Photonic Crystals. *Proc. Natl. Acad. Sci. U. S. A.* **2012**, *109*, 14332−14336.
(10) Matranga, A.; Baig, S.; Boland, J.; Newton, C.; Taphouse, T.; Wells, G.; Kitson, S. Biomimetic Reflectors Fabricated Using Self-Organising, Self-Aligning Liquid Crystal Polymers. *Adv. Mater.* **2013**, *25*, 520−523.
(11) Li, Y.; Prince, E.; Cho, S.; Salari, A.; Golestani, Y. M.; Lavrentovich, O. D.; Kumacheva, E. Periodic Assembly of Nanoparticle Arrays in Disclinations of Cholesteric Liquid Crystals. *Proc. Natl. Acad. Sci. U. S. A.* **2017**, *114*, 2137−2142.
(12) Jensen, J.; Grundy, S. C.; Bretz, S. L.; Hartley, C. S. Synthesis and Characterization of Self-assembled Liquid Crystals: p-alkoxybenzoic acids. *J. Chem. Educ.* **2011**, *88*, 1133−1136.
(13) Kim, J. G.; Park, S. Y. Photonic Spring-Like Shell Templated from Cholesteric Liquid Crystal Prepared by Microfluidics. *Adv. Opt. Mater.* **2017**, *5*, 1700243−1700251.
(14) Hussain, S.; Park, S. Y. Optical Glucose Biosensor Based on Photonic Interpenetrating Polymer Network with Solid-state Cholesteric Liquid Crystal and Cationic Polyelectrolyte. *Sens. Actuators B Chem.* **2020**, 128099−128109.
(15) Munir, S.; Hussain, S.; Park, S. Y. Patterned Photonic Array Based on an Intertwined Polymer Network Functionalized with a Nonenzymatic Moiety for the Visual Detection of Glucose. *ACS Appl. Mater. Interfaces* **2019**, *11*, 37434−37441.
(16) Noh, K. G.; Park, S. Y. Smart Molecular-spring Photonic Droplets. *Mater. Horiz.* **2017**, *4*, 633−640.
(17) Khan, M.; Park, S. Y. Glucose Biosensor Based on GOx/HRP bienzyme at Liquid−crystal/Aqueous Interface. *J. Colloid Interface Sci.* **2015**, *457*, 281−288.
(18) Myung, D.-b.; Hussain, S.; Park, S. Y. Photonic Calcium and Humidity Array Sensor Prepared with Reactive Cholesteric Liquid Crystal Mesogens. *Sens. Actuators B Chem.* **2019**, *298*, 126894−126903.
(19) Noh, K. G.; Park, S. Y. Biosensor Array of Interpenetrating Polymer Network with Photonic Film Templated from Reactive Cholesteric Liquid Crystal and Enzyme-Immobilized Hydrogel Polymer. *Adv. Funct. Mater.* **2018**, *28*, 1707562−1707571.
(20) Kim, B.; Kang, B.; Vales, T. P.; Yang, S. K.; Lee, J.; Kim, H. J. Polyphenol-functionalized Hydrogels Using an Interpenetrating Chitosan Network and Investigation of Their Antioxidant Activity. *Macromol. Res.* **2018**, *26*, 35−39.
(21) Vales, T. P.; Badon, I. W. T.; Kim, H. J. Multi-responsive Hydrogels Functionalized with a Photochromic Spiropyran-conjugated Chitosan Network. *Macromol. Res.* **2018**, *26*, 950−953.
(22) Munir, S.; Khan, M.; Park, S. Y. Bienzyme Liquid-crystal-based Cholesterol Biosensor. *Macromol. Res.* **2015**, *220*, 508−515.
(23) Zhang, J.; Gai, M.; Ignatov, A. V.; Dyakov, S. A.; Wang, J.; Gippius, N. A.; Frueh, J.; Sukhorukov, G. B. Stimuli-Responsive Microarray Films for Real-Time Sensing of Surrounding Media, Temperature, and Solution Proper-ties via Diffraction Patterns. *ACS Appl. Mater. Interfaces* **2020**, *12*, 19080−19091.
(24) Zhang, J.; Sun, R.; DeSouza-Edwards, A. O.; Frueh, J.; Sukhorukov, G. B. Microchamber Arrays Made of Biodegradable Polymers for Enzymatic Release of Small Hydrophilic Cargos. *Soft Matter* **2020**, *16*, 2266−2275.

(25) Ko, Y.; Jeong, H. Y.; Kwon, G.; Kim, D.; Lee, C.; You, J. pH-Responsive Polyaniline/Polyethylene glycol Composite Arrays for Colorimetric Sensor Application. *Sens. Actuators B Chem* **2020**, *305*, 127447−127455.
(26) Gao, W.; Emaminejad, S.; Nyein, H. Y. Y.; Challa, S.; Chen, K.; Peck, A.; Fahad, H. M.; Ota, H.; Shiraki, H.; Kiriya, D.; Lien, D.-H.; Brooks, G. A.; Davis, R. W.; Javey, A. Fully Integrated Wearable Sensor Arrays for Multiplexed in Situ Perspiration Analysis. *Nature* **2016**, *529*, 509−514.
(27) Hauke, A.; Simmers, P.; Ojha, Y. R.; Cameron, B. D.; Ballweg, R.; Zhang, T.; Twine, N.; Brothers, M.; Gomez, E.; Heikenfeld, J. Complete Validation of a Continuous and Blood-correlated Sweat Biosensing Device with Integrated Sweat Stimulation. *Lab Chip* **2018**, *18*, 3750−3759.
(28) Moirangthem, M.; Arts, R.; Merkx, M.; Schenning, A. P. H. J. An Optical Sensor Based on a Photonic Polymer Film to Detect Calcium in Serum. *Adv. Funct. Mater.* **2016**, *26*, 1154−1160.
(29) Dudev, T.; Lim, C. The effect of Metal Binding on the Characteristic Infrared Band Intensities of Ligands of Biological Interest. *J. Mol. Struct.* **2012**, *1009*, 83−88.
(30) Nara, M.; Morii, H.; Tanokura, M. Coordination to Divalent Cations by Calcium-binding Proteins Studied by FTIR Spectroscopy. *Biochim. Biophys. Acta, Biomembr.* **2013**, *1828*, 2319−2327.
(31) Bala, T.; Prasad, B. L. V.; Sastry, M.; Kahaly, M. U.; Waghmare, U. V. Interaction of Different Metal Ions with Carboxylic Acid Group: a quantitative study. *J. Phys. Chem. A* **2007**, *111*, 6183−6190.
(32) Lee, S. S.; Kim, B.; Kim, S. K.; Won, J. C.; Kim, Y. H.; Kim, S. H. Robust Microfluidic Encapsulation of Cholesteric Liquid Crystals toward Photonic Ink Capsules. *Adv. Mater.* **2015**, *27*, 627−633.
(33) Uchida, Y.; Takanishi, Y.; Yamamoto, J. Controlled Fabrication and Photonic Structure of Cholesteric Liquid Crystalline Shells. *Adv. Mater.* **2013**, *25*, 3234−3237.
(34) Shrestha, V. R.; Park, C.-S.; Lee, S. S. Enhancement of Color Saturation and Color Gamut Enabled by a Dual-band Color Filter Exhibiting an Adjustable Spectral Response. *Opt. Express* **2014**, *22*, 3691−3704.
(35) Zehentbauer, F. M.; Moretto, C.; Stephen, R.; Thevar, T.; Gilchrist, J. R.; Pokrajac, D.; Richard, K. L.; Kiefer, J. Spectroscopy, B. Fluorescence Spectroscopy of Rhodamine 6G: Concentration and Solvent Effects. *Spectrochim. Acta A Mol. Biomol. Spectrosc.* **2014**, *121*, 147−151.
(36) Huang, C. T.; Chen, M. L.; Huang, L. L.; Mao, I. F. Uric Acid and Urea in Human Sweat. *Chin. J. Physiol.* **2002**, *45*, 109−116.
(37) Gowda, S.; Desai, P. B.; Kulkarni, S. S.; Hull, V. V.; Math, A. A. K.; Vernekar, S. N. Markers of Renal Function Tests. *North Am. J. Med. Sci.* **2010**, *2*, 170.
(38) Liu, L.; Mo, H.; Wei, S.; Raftery, D. Quantitative Analysis of Urea in Human Urine and Serum by ^{1}H Nuclear Magnetic Resonance. *Analyst* **2012**, *137*, 595−600.
(39) Danaei, G.; Finucane, M. M.; Lu, Y.; Singh, G. M.; Cowan, M. J.; Paciorek, C. J.; Lin, J. K.; Farzadfar, F.; Khang, Y. H.; Stevens, G. A.; Rao, M.; Ali, M. K.; Riley, L. M.; Robinson, C. A.; Ezzati, M. National, Regional, and Global trends in Fasting Plasma Glucose and Diabetes Prevalence since 1980: Systematic Analysis of Health Examination Surveys and Epidemiological Studies with 370 Country-years and 2·7 Million Participants. *Lancet* **2011**, *378*, 31−40.
(40) Ma, J.; Yan, L.; Guo, T.; Yang, S.; Liu, Y.; Xie, Q.; Ni, D.; Wang, J. Association Between Serum Essential Metal Elements and the Risk of Schizophrenia in China. *Sci. Rep.* **2020**, *10*, 10875.
(41) Huynh, U. T. D.; Lerbret, A.; Neiers, F.; Chambin, O.; Assifaoui, A. Binding of Divalent Cations to Polygalacturonate: A Mechanism Driven by the Hydration Water. *J. Phys. Chem. B.* **2016**, *120*, 1021−1032.
(42) Malovíková, A.; Rinaudo, M.; Milas, M. Comparative Interactions of Magnesium and Calcium Counterions with Poly-galacturonic Acid. *Biopolymers* **1994**, *34*, 1059−1064.
(43) Ederth, T.; Claesson, P. M. Forces between Carboxylic Acid Surfaces in Divalent Electrolyte Solutions. *J. Colloid Interface Sci.* **2000**, *229*, 123−128.

https://dx.doi.org/10.1021/acsami.0c15718
ACS Appl. Mater. Interfaces XXXX, XXX, XXX−XXX